Acta Cryst. (1999). A**55**, 84–94

On the prediction of crystal morphology. III. Equilibrium and growth behaviour of crystal faces containing multiple connected nets

R. F. P. Grimbergen, P. Bennema and H. Meekes*

RIM Laboratory of Solid State Chemistry, Faculty of Science, University of Nijmegen, Toernooiveld 1, 6525 ED Nijmegen, The Netherlands. E-mail: hugom@sci.kun.nl

(*Received 5 March 1998; accepted 29 June 1998*)

Abstract

In this paper, the equilibrium and growth behaviour of faces (*hkl*) with more than one connected net is studied. It is shown that for these types of orientation different surface phases exist under equilibrium conditions as a function of temperature. Depending on the exact bonding topology at the surface, flat, rough or disordered flat phases are found. Moreover, the growth rate R_{hkl} of such faces can differ significantly from the usually calculated relative growth rates based on the attachment energy. Monte Carlo simulations confirm the results from the Hartman–Perdok analyses and offer a tool for the prediction of the crystal habit as a function of supersaturation.

1. Introduction

Recently, a physical foundation for the description of the stability of faces (*hkl*) of crystals in terms of connected nets and periodic bond chains (PBCs) was derived (Grimbergen, Meekes, Bennema, Strom & Vogels, 1998). It was shown that application of the PBC theory to a crystal structure often leads to many connected nets for an orientation (*hkl*) and that specific combinations of connected nets may even cause a face (*hkl*) to roughen at 0 K ($T^R = 0$). This phenomenon was called symmetry roughening and it can have major implications for crystal morphology.

In a second paper (Meekes *et al.*, 1998), all relevant symmetry relations for pairs of connected nets of a single orientation (*hkl*) were analysed. It was found that some symmetry relations between connected nets cause symmetry roughening and others result in the classical Bravais–Friedel–Donnay–Harker (BFDH) selection rules. The influence of a mother phase in contact with the crystal was included in the analysis.

In the present paper, besides crystal faces containing symmetry-related pairs of connected nets, we also treat pairs of connected nets for which such a symmetry relation is not present. The present approach is not the only one that takes (pseudo-) symmetry into account. In particular, the reader is referred to the work of Follner (1988). It will be shown, however, that despite the absence of a symmetry relation the effective step free energy can be very low resulting in what will be called pseudo-symmetry roughening. In this paper, simple crystal surface models, which are in our opinion generic for many types of crystal, will be used to illustrate the equilibrium and growth behaviour of a crystal face as a function of the connected net structure. In some cases, the presence of multiple connected nets gives rise to a very small step energy which results in a roughening temperature for the orientation (*hkl*) (T^R_{hkl}) lower than the calculated two-dimensional Ising transition temperature (T^C_{hkl}) based on the connected net with the highest slice energy (Grimbergen, Meekes, Bennema, Strom & Vogels, 1998). For other cases, a so-called disordered flat (DOF) phase is found which is known from simple statistical thermodynamical surface models with next-nearest-neighbour interactions (Rommelse & den Nijs, 1987; den Nijs & Rommelse, 1989). Recently, DOF phases were found for the (111) (Woodraska & Jaszczak, 1997*a*,*b*) and (100) (den Nijs, 1997) faces of silicon and there is experimental (Grimbergen, Reedijk *et al.*, 1998) and theoretical (Grimbergen, Meekes, Bennema, Knops & den Nijs, 1998) evidence that a DOF phase exists for the (011) faces of naphthalene.

Obviously, the surface phase of a face (*hkl*) will also affect the growth rate and mechanism of that face. It is well known that the step free energy is an important parameter that determines the growth rate to a large extent. In the flat phase, the step free energy is larger than zero and at low supersaturations layer-by-layer growth occurs, whereas in the rough phase the step free energy has vanished and continuous (rough) growth occurs even at the lowest supersaturations. For a DOF phase, the step free energy has vanished, but a difference in energy of crossing steps keeps the surface flat. The effective nucleation barrier in the DOF phase appears to be very small (Woodraska & Jaszczak, 1997*a*,*b*; Grimbergen, Meekes, Bennema, Knops & den Nijs, 1998).

In general, we will show that crystal faces containing multiple connected nets may have a very small effective step energy which results in the growth rate being higher than the traditionally calculated growth rate which assumes a rate proportional to the attachment energy.

ISSN 0108-7673

The qualitative results are verified by Monte Carlo (MC) simulations of these specific orientations under equilibrium and growth conditions. In this way, a prediction of the crystal habit as a function of temperature and supersaturation can be achieved. Note that the morphology based on the attachment energy is by definition independent of the supersaturation (Hartman & Bennema, 1980). In this paper, ideal crystal structures are treated which grow by a two-dimensional nucleation mechanism. The effects of impurities or defects are not explicitly taken into account.

In the following section, three model crystal graphs are introduced. For all models, the (001) orientation consists of multiple connected nets. In §3, the connected-net analysis for the (001) faces of all models is presented and the roughening transition temperatures are estimated. In addition, the growth behaviour will be discussed. In §4, the MC simulation results are presented and, in §5, the MC results are compared with the results of the connected-net analysis and the growth morphology is derived. Moreover, from the simulation data, the growth morphology as a function of supersaturation is predicted. Finally, in §6, some conclusions are drawn.

2. Model crystal graphs

In this section, three different types of crystal graph are introduced which are generic for many crystals. The attention will be focused on the (001) orientation of these graphs. All (001) orientations have in common that there are at least two different connected nets present. The number of growth units in the unit cell of all crystal graphs is two ($Z = 2$). Growth units are labelled A and B to indicate that their position with respect to the (001) orientation may be different. It is assumed that the chemical composition of the growth units is equivalent. In a crystal graph, growth units are represented by points. Therefore, a crystal graph generally has a higher symmetry than the corresponding crystal and bonds in the crystal graph which are apparently the same can be different due to the space-group symmetry of the crystal.

The first crystal graph is shown in Fig. 1. The (001) orientation can be considered as that of a classical simple cubic or Kossel crystal. However, the difference is that in our model the (001) face is an AB-layered structure. Two different types of crystal surface were studied for the (001) face of this crystal graph. The first type has equivalent horizontal bonds and thus the bond energies are equal ($\Phi_a = \Phi_b$) and the vertical bonds are different ($\Phi_c \neq \Phi_d$), Φ being the bond energy per growth unit. In this case, we consider a layered structure with alternating layers A and B with vertical bonds c and d, respectively. This surface type will be referred to as type I. Second, the case where the vertical bonds are equivalent ($\Phi_c = \Phi_d$) and the horizontal bonds differ ($\Phi_a \neq \Phi_b$) is considered. This type of crystal face is called type II. Note that in the isotropic case with $\Phi_a = \Phi_b = \Phi_c = \Phi_d$ the two types I and II become equivalent and correspond to the well studied (001) face of the Kossel model.

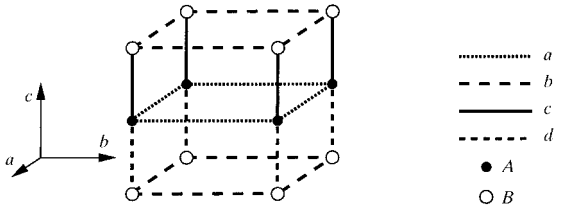

Fig. 1. Crystal graph for the AB-layered Kossel models (types I and II).

The second model graph of which the (001) orientation corresponds to a (110) Kossel-like face is shown in Fig. 2. Again, it is clear that this orientation is an AB-layered structure. Along the a direction, a horizontal bond a is present, whereas in the b direction there is no horizontal bond present. The oblique bonds p and q make the crystal graph connected. This type of crystal surface is called type III.

To study (001) AB-layered body-centred types of crystal surface, the (001) face of a third model graph depicted in Fig. 3 was used. Note that there are no horizontal bonds present for the (001) orientation neither in the a nor in the b direction, but exclusively the oblique bonds p and q. This type of crystal facet is called type IV.

3. Connected-net analysis

In the following subsections, all connected nets for the (001) orientations of the model crystal graphs will be presented briefly. All connected nets are used to derive the overall broken-bond step energies.

3.1. *Types I and II*

Four connected nets can be identified for the (001) orientation of the crystal graph in Fig. 1. A [100] projection of the connected nets is shown in Fig. 4. From the figure, it can be clearly observed that the connected nets $(001)_1$ and $(001)_2$ consist of two stacked $(001)_3$ and

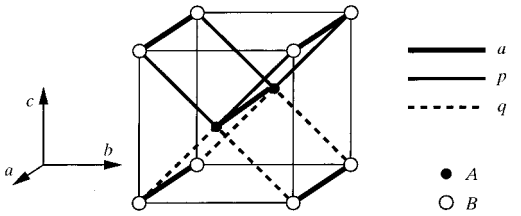

Fig. 2. Crystal graph for the modified (110) Kossel model (type III). The thin solid lines are drawn to indicate the unit-cell edges but do not represent bonds of the crystal graph.

$(001)_4$ connected nets. The broken-bond step energy for this orientation is equal to the step energy of a step $(001)_1$ [or $(001)_2$] for both types I and II and is equal to $(\gamma_1 + \gamma_2)$ in both the *a* and *b* directions. This step energy determines the roughening transition temperature T^R_{001}. In the special case that $\Phi_a = \Phi_b = \Phi_c = \Phi_d = \Phi$, the roughening temperature will be governed by γ_1 $(= \gamma_2 = \Phi)$. Again, this limiting case corresponds to the (001) face of the simple cubic Kossel model. A type I facet grows with either $(001)_1$ or $(001)_2$ growth layers depending on the surface free energy of the surface bounded by $(001)_1$ or $(001)_2$. In principle, the orientation can grow alternately with $(001)_3$ and $(001)_4$ growth layers when the energies do not differ too much. Type II surfaces will grow alternately with layers $(001)_3$ and $(001)_4$. Usually, it is assumed that the growth rate will be determined mainly by the layer with the lowest growth velocity.

3.2. *Type III*

The (001) face of the crystal graph in Fig. 2 contains two connected nets $(001)_1$ and $(001)_2$. In Fig. 5, the [100] projection of the connected nets is depicted. Assuming that $\Phi_p < \Phi_q$, the (001) face will be bounded by $(001)_1$. The step energy is equal to the broken-bond step energy, γ_1. This step energy can be found by calculating the energy difference of the surface bounded by $\alpha\beta\gamma\delta$ and $\alpha\beta\varepsilon\varphi\gamma\delta$ (Fig. 5) (Grimbergen, Meekes, Bennema, Strom & Vogels, 1998). For this case, $\gamma_1 = \Phi_q - \Phi_p$ for both step $\beta\varepsilon$ and step $\varphi\gamma$. Note that the broken-bond step energy along the [010] direction is equal to the broken-bond energy, Φ_a. The growth kinetics for these types of crystal facet are governed by the broken-bond energy difference $|\Phi_p - \Phi_q|$. If $|\Phi_p - \Phi_q| \to 0$, the step free energy will become very small. Therefore, it is expected that the crystal facet becomes rough at very low supersaturations and will grow in a rough (continuous) mode [$R_{hkl} \propto \exp(\Delta\mu)$]. A limiting case is the situation where $\Phi_p = \Phi_q$. Then the model reduces to the (110) face of a simple cubic Kossel model which has a roughening temperature of 0 K. Note that for that case formally no valid connected net is present for this orientation (Grimbergen, Meekes, Bennema, Strom & Vogels, 1998). Consequently, such a facet will grow in a continuous (rough) mode and is in fact already rough at zero supersaturation.

3.3. *Type IV*

Principally, the same situation described in the previous subsection applies to the (001) orientation of the crystal graph of Fig. 3. The fundamental difference between faces of type III and type IV is that for type IV the broken-bond step energies for the [100] and [010] directions are equal to the step energies of type III faces along the [100] direction. This step energy is equal to $|\Phi_p - \Phi_q|$ and determines the roughening transition temperature for type IV facets. Under growth conditions, the two-dimensional nucleation barrier is determined only by the step energy $|\Phi_p - \Phi_q|$.

A well known limiting case for which $\Phi_p = \Phi_q$ is described by the isotropic BCSOS model without next-nearest-neighbour interactions (van Beijeren, 1977). This model has a roughening transition temperature (T^R) of 0 K.

4. Monte Carlo simulations

4.1. *Simulation set-up*

For all simulations, a standard metropolis algorithm was implemented. The rate of attachment of molecules at a site (K^+) is proportional to the supersaturation $\Delta\mu$,

$$K^+(\Delta\mu) = K_0^+ \exp[\Delta\mu/kT], \tag{1}$$

where *k* is the Boltzmann constant and *T* is the absolute temperature. K_0^+ is the attachment rate at equilibrium given by

$$K_0^+ = P_0^+ I_0 A, \tag{2}$$

where P_0^+ is the probability that a growth unit impinging on a site is correctly positioned to attach to the crystal surface, I_0 is the equilibrium rate of impingement of growth units per unit area and *A* is the area of a lattice site. In our simulation, we assume that P_0^+ is not dependent on the type of bond that is being formed and is taken to be a constant (Gilmer & Jackson, 1977). For our *AB*-layered surfaces, the rate at which growth units at the surface will detach depends exponentially on the

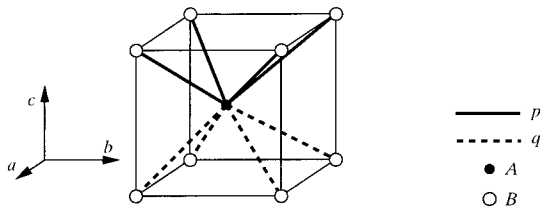

Fig. 3. Crystal graph for the (001) BCSOS model (type IV). The thin solid lines are drawn to indicate the edges of the unit cell, but do not represent bonds of the crystal graph.

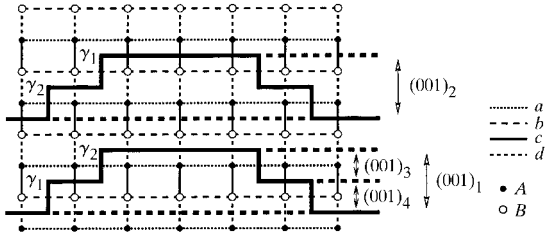

Fig. 4. Projection along [100] of the crystal graph in Fig. 1. Connected nets are indicated with $(hkl)_n$ with $n = 1, 2, 3, 4$. The broken-bond step energies γ_1 and γ_2 are also shown.

binding energy (E_b^A for layer A and E_b^B for layer B) of the growth unit at the surface, which is strongly site dependent,

$$K^-(E_b^A/kT) = K_0^- \exp[-E_b^A/kT] \tag{3}$$

and

$$K^-(E_b^B/kT) = K_0^- \exp[-E_b^B/kT], \tag{4}$$

where K_0^- is a constant. At equilibrium, the average detachment and attachment rates must be equal. For our layered surface structures, we have assumed that the average attachment rate is equal to the average detachment rate of a growth unit with a binding energy of exactly half of the average binding energy of a growth unit in the fully occupied lattice, denoted $\bar{\Phi}$,

$$K^+(\Delta\mu = 0) = K^-(\bar{\Phi}/kT). \tag{5}$$

This implies, along with (1), the relation

$$K_0^+ = K_0^- \exp[\mu_0/kT], \tag{6}$$

where $\mu_0 = -\bar{\Phi}$ is the average chemical potential at equilibrium. In our simulation model, the anisotropy (δ) is defined in terms of bond energies Φ according to

$$\delta = (\Phi_1/\Phi_2) \wedge [(\Phi_1 + \Phi_2)/2] = \Phi, \tag{7}$$

with $0 < \delta \leq 1$. Relation (7) guarantees a constant lattice energy for simulations with a different anisotropy. The definition of the bonds used in the MC simulations of the four types of crystal facet are listed in Table 1. Note that bond energies are defined per growth unit (Φ) while in the simulation the total energy of a bond (2Φ) is used. Our simulation model has three free (dimensionless) parameters, namely Φ/kT, δ and $\Delta\mu/kT$.

The solid-on-solid (SOS) condition was defined differently for the different types of surface. For type I and II faces, the standard SOS condition of the simple cubic Kossel model was applied for which all incoming growth units can only be bonded to an underlying growth unit (c or d bond, see Fig. 1). A modified SOS condition has been applied for type III faces. Each incoming growth unit has to make two bonds with the interface (either p or q bonds, see Fig. 2). For the type IV faces, four bonds (either p or q, see Fig. 3) have to be formed. This is the well known BCSOS condition.

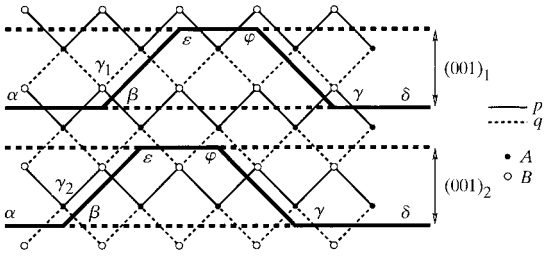

Fig. 5. Projection along [100] of the crystal graph in Fig. 2 and the crystal graph in Fig. 3. Connected nets are indicated with $(hkl)_n$ with $n = 1, 2$.

Table 1. *Definitions of bonds used in the MC simulations for the different model types I–IV*

In the second and third columns, the bonds that lead to the anisotropy (Φ_1 and Φ_2) are given for each model. The remaining bonds of each model are shown in the fourth column and have a bond strength of Φ per growth unit in our simulation model. In the fifth column, half of the average binding energy of a growth unit in the fully occupied lattice is given and the last two columns contain the binding energies for a growth unit in layer A or B with number of neighbours i within the layer. Note that for the model types I and II i = 0–4 and for type III i = 0–2. For model IV, the binding energy at a site does not depend on the number of neighbours.

Type	Φ_1	Φ_2	Φ	$\bar{\Phi}$	E_b^A	E_b^B
I	Φ_c	Φ_d	Φ_a, Φ_b	6Φ	$-2\Phi_1 - 2i\Phi$	$-2\Phi_2 - 2i\Phi$
II	Φ_a	Φ_b	Φ_c, Φ_d	6Φ	$-2\Phi - 2i\Phi_1$	$-2\Phi - 2i\Phi_2$
III	Φ_p	Φ_q	Φ_a	6Φ	$-4\Phi_1 - 2i\Phi$	$-4\Phi_2 - 2i\Phi$
IV	Φ_p	Φ_q	–	8Φ	$-8\Phi_1$	$-8\Phi_2$

Sticking coefficients, S, for the surfaces were defined as

$$S = \frac{\text{attachments} - \text{removals}}{\text{attachment attempts}}, \tag{8}$$

and crystal growth rates, R, by

$$R = Sd_{hkl}K^+, \tag{9}$$

where d_{hkl} is the interplanar distance of the face (hkl).

A convenient unit of time used in MC simulations is the Monte Carlo sweep (MCS), which is unity when the number of attempted moves is equal to the number of matrix sites. In our simulations, square matrices with dimensions 30×30 ($L = 30$) and 40×40 ($L = 40$) were used. The equilibration time was typically of the order of 1×10^5–0.5×10^6 MCS and the subsequent data collection run 0.5×10^6–1×10^6 MCS. For the anisotropy parameter, the values $\delta = 1$, 0.8, 0.6 and 0.4 were chosen.

During the simulation, several quantities were calculated. A very important quantity is the height-difference correlation function, which diverges in the case of thermal roughening [for a review see Weeks (1986) and van Beijeren & Nolden (1986)]. The height-difference correlation function is defined as

$$G(r) \equiv \langle [h(r) - h(r_0)]^2 \rangle \tag{10}$$

and diverges in the case of thermal roughening as

$$\lim_{r\to\infty} G(r)/a^2 \to [K_\infty(T)/\pi] \ln(r). \tag{11}$$

Here, $h(r_0)$ is the height of a reference position, $r = |r - r_0|$ is the lateral distance parallel to the surface, a is the vertical periodicity and $\langle \ldots \rangle$ denotes a thermal average. The roughening temperature can be determined by locating the temperature at which the $G(r)$ function takes on the universal value $K_\infty = 2/\pi$ (Shugard *et al.*, 1978). For our models, the periodicity is

Table 2. *Results of the Monte Carlo simulations for* $\Delta\mu = 0$

For all four types of surface, the temperatures kT/Φ are listed where the specific heat $c(T)$ has a maximum and the amplitude A of the height-difference correlation function $G(r)$ becomes 2 ($\delta = 1$) or 8 ($\delta < 1$) as a function of the anisotropy δ.

	Type I		Type II		Type III		Type IV	
δ	$c(T)$ (kT/Φ)	$G(r)$ (kT/Φ)	$c(T)$ (kT/Φ)	$G(r)$ (kT/Φ)	$c(T)$ (kT/Φ)	$G(r)$ (kT/Φ)	$c(T)$ (kT/Φ)	$G(r)$ (kT/Φ)
0.4	1.74	2.22	2.10	2.41	1.40	3.10	1.25	–
0.6	1.60	2.22	1.90	2.35	1.05	2.90	0.67	–
0.8	1.33	2.22	1.74	2.25	0.70	2.65	0.31	–
1.0	1.17	1.29	1.17	1.29	–	–	–	–

$a = 2$ [equation (11)] for the case $\delta < 1$ due to the AB-layered structure. For $\delta = 1$, the periodicity is a single layer and thus $a = 1$ was used in (11) to determine the roughening temperature. The height-difference simulation data were fitted to the functional form $G(r) = [A/\pi^2]\ln(r) + C$ for $L = 40$ and $r = 6$–16. Note that, for $\delta = 1$, thermal roughening occurs for the case $A \geq 2$ and, for $\delta < 1$, roughening occurs for $A \geq 8$.

Another quantity that can be calculated easily during the MC simulation is the surface specific heat $c(T)$. The surface specific heat can be calculated from the surface energy fluctuations as

$$c(T) = (1/NkT^2)(\langle E_s^2\rangle - \langle E_s\rangle^2), \tag{12}$$

where N is the number of matrix sites, k is the Boltzmann constant, T is the absolute temperature and E_s is the surface energy of the complete surface. Because of its sensitivity to energy fluctuations in finite systems, $c(T)$ is a useful tool for indicating phase transitions.

The interface width $\langle \delta h^2\rangle^{1/2}$ provides information on the roughness of a crystal face and is defined as

$$\langle \delta h^2\rangle \equiv (1/N)\sum_i \langle (h_i - \bar{h})^2\rangle, \tag{13}$$

where N is the number of matrix sites and

$$\bar{h} = (1/N)\sum_i h_i. \tag{14}$$

4.2. *Equilibrium results*

In Table 2, the results of the equilibrium MC simulations for the four types of (001) facets are summarized.

4.2.1. *Types I and II*. The results for types I and II are comparable. At low temperatures, the facets are perfectly flat whereas at higher temperatures first excitations of single particles appear and eventually the face becomes completely rough at high temperatures. As already mentioned before, in the isotropic limit $\delta = 1$, type I and II both represent the simple cubic Kossel model. The Monte Carlo results for this case yield a roughening temperature of $kT^R/\Phi = 1.29$, which is in good agreement with previously reported values of $kT^R/\Phi = 1.28$ (Leamy & Gilmer, 1974). Moreover, the maximum in the specific heat at $kT/\Phi = 1.17$ is in good agreement with the reported value of $kT/\Phi = 1.15$ by Swendsen (1977).

From the connected-net analysis in §3, it was concluded that the roughening temperatures T^R of type I and II surfaces are determined by the overall step energy of a complete step (001). With the restrictions of our MC simulations [see equation (7)], this step energy is for both types equal to $\Phi = 2kT$ for the case $\delta < 1$. As an estimate for the roughening temperature T^R, the two-dimensional Ising transition temperature T^C of a simple cubic isotropic connected net with a bond strength of 2Φ can be calculated. Using the program *TCRITIC* (Hoeks, 1993), we found $kT^C/\Phi = 2.27$, which is in rather good agreement with the calculated roughening temperatures for the type I and II surfaces determined from the height-difference correlation function $G(r)$ as shown in Table 2.

At the temperature at which the specific heat has a maximum, the fluctuations of the surface energy are maximal. The specific heat for type II surfaces is plotted against the temperature in Fig. 6. We attribute the increase in fluctuations to a drastic drop in the step free energy of the strongest connected net $(001)_3$ (for the case $\Phi_a > \Phi_b$, see Fig. 4) which is present at the surface. On the other hand, the roughening temperature has a value that is considerably higher than the maximum in

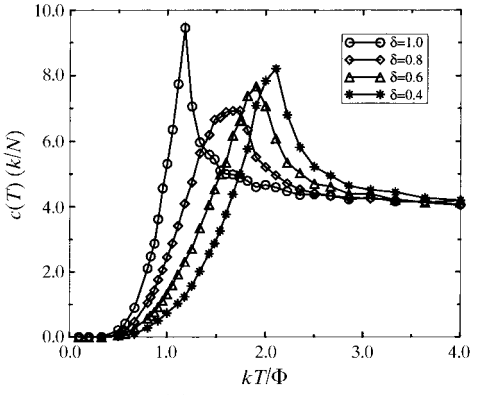

Fig. 6. The specific heat $c(T)$ for type II surfaces as a function of the temperature kT/Φ for δ = 1.0, 0.8, 0.6 and 0.4.

$c(T)$. Moreover, T^R is less dependent on the anisotropy, at least for type I. The temperature interval between $T(c^{\max})$ and T^R is rather small in the isotropic case, takes on the largest value for very small anisotropy and decreases again for larger anisotropies. In Fig. 7, the interface width δh for type II surfaces is plotted. Remarkably, in the anisotropic cases the interface width becomes more or less linear at $T = T^R$. Moreover, the deviation for the anisotropic cases from the isotropic surface, starting from $\Delta\mu/kT \simeq 1$, clearly demonstrates that the anisotropic surfaces maintain their flatness up to higher temperatures. The difference in behaviour of the isotropic surface and the slightly anisotropic surface ($\delta = 0.8$) indicates that the introduction of anisotropy has an unexpectedly pronounced effect. All these observations suggest that for anisotropic AB-layered Kossel-like faces the surface becomes locally disordered but remains essentially flat at temperatures between $T(c^{\max})$ and T^R. This intermediate phase might be compared with that of a DOF phase, although such a phase has not been identified for such types of surface.

In order to gain more insight into the behaviour of the step energy as a function of temperature, simulations were performed for type II surfaces with and without a complete step along [010]. This was performed by a modification in the periodic boundary conditions in such a way that a complete (001) step (with height 2 due to the AB-layered structure) is always present. From these simulations the step energy densities for $\delta = 1.0$, $\delta = 0.8$ and $\delta = 0.6$ were calculated as shown in Fig. 8. If the results are compared with Table 2, it is clear that the step energy drops drastically at the temperature $T(c^{\max})$ and slowly approaches zero at T^R. Thus, the steepness of the step energy density drop is a measure of the temperature interval for the intermediate phase. The drop in step energy can also be found in simulated growth curves which will be presented in §4.3.

4.2.2. *Type III*. Recently, the phase diagram of type III surfaces was derived showing a flat, a disordered flat (DOF) and a rough phase. It was shown that the temperature at which a maximum in the specific heat is found coincides with the pre-roughening transition temperature $T^{\rm pr}$ (Grimbergen, Meekes, Bennema, Knops & den Nijs, 1998). The roughening transition at $T = T^R$ was found at the point where the amplitude A became larger than 8. The MC results of the present study are equivalent to those presented by Grimbergen, Meekes, Bennema, Knops & den Nijs (1998). It can be concluded that type III surfaces are flat for $T < T^{\rm pr}$, disordered flat for $T^{\rm pr} < T < T^R$ and rough for $T > T^R$. At $T = T^{\rm pr}$, the step energy drops to a very small value. This behaviour of the step energy as a function of temperature can be compared with the results for type II surfaces as shown in Fig. 8. The case of $\delta = 1$ is absent in Table 2 because it corresponds to the anisotropic limit of the model for which the step energy along the [100] direction (see Fig. 5) is zero. Therefore, the roughening temperature kT^R/Φ is zero. It is not possible to perform a reliable MC simulation for this limiting case.

4.2.3. *Type IV*. The results for type IV surfaces with $\delta = 1$ are rather trivial since the step energies for both the [100] and [010] direction are zero. This isotropic case has a roughening temperature of 0 K (van Beijeren, 1977). For the case $\delta < 1$, the step energy is larger than zero. A remarkable feature of the MC results for $\delta < 1$ is that the amplitude A does not exceed the critical value of 8, even at the highest temperatures, indicating that the surface does not become rough (Table 2). In our opinion, the results of the type IV surface model can be compared with those of the staggered BCSOS model as described by Mazzeo *et al.* (1995) and Nolden & van Beijeren (1994), where for anisotropic surfaces with attractive bonds only a flat and a DOF phase were found. Therefore, we think that our model has a flat and a DOF phase separated by a pre-roughening phase transition which causes the maximum in the specific heat. The absence of a rough phase must be attributed to the very strict solid-on-solid condition. The tempera-

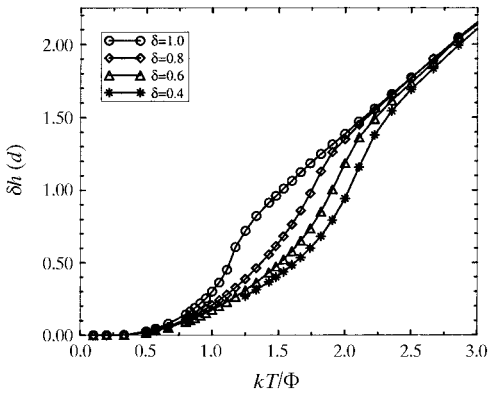

Fig. 7. Interface width δh for type II surfaces as a function of temperature.

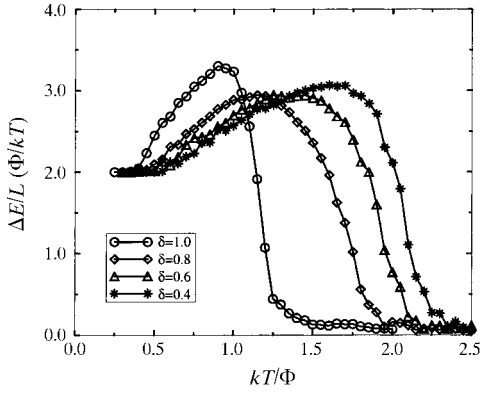

Fig. 8. Step energy density $\Delta E/L$ for type II surfaces as a function of the temperature kT/Φ for δ = 1.0 (kT^R/Φ = 1.29), 0.8 (kT^R/Φ = 2.25) and 0.6 (kT^R/Φ = 2.35).

tures at which the specific heat is maximal are in good agreement with the calculated two-dimensional Ising transition temperature of a simple cubic isotropic connected net with a bond strength equal to the effective step energy ($\Phi_p - \Phi_q$) calculated using the program *TCRITIC* (Hoeks, 1993). The calculated two-dimensional Ising transition temperatures were $kT^C/\Phi = 1.10$ ($\delta = 0.4$), $kT^C/\Phi = 0.64$ ($\delta = 0.6$) and $kT^C/\Phi = 0.28$ ($\delta = 0.8$).

4.3. *Off-equilibrium results*

In order to study the growth behaviour of the different types of crystal face, MC simulations with $\Delta\mu/kT > 0$ were performed. In the present study, we restricted ourselves to simulations of perfect crystal facets without dislocations. Thus, the growth mechanism is two-dimensional nucleation growth at low supersaturation and continuous (rough) growth at higher supersaturations.

4.3.1. *Types I and II*. For the type I surfaces, the surface (or attachment) energies for the two sublayers A and B become different for the case $\delta < 1$. It is expected that upon increasing the anisotropy ($\delta \to 0$) the growth rate will decrease as the attachment energy for a complete double layer (001) decreases. The results of the MC simulations are shown in Fig. 9. The temperature $kT/\Phi = 0.83$ is chosen in such a way that all surfaces are flat at $\Delta\mu = 0$. It can be seen very clearly that the nucleation barrier increases with decreasing δ (*i.e.* increasing anisotropy). An interesting detail in Fig. 9 is the behaviour of the sticking fraction for the isotropic ($\delta = 1$) surface as compared with the behaviour of the sticking fraction for small anisotropy ($\delta = 0.8$). It is clear that, when the anisotropic face starts growing ($\Delta\mu = 0.45kT$), it is almost immediately growing linearly with increasing supersaturation. In contrast, the isotropic ($\delta = 1$) surface starts growing at much lower supersaturation ($\Delta\mu/kT = 0.17$) and becomes linear at much higher supersaturation ($\Delta\mu/kT \simeq 0.9$). At $\Delta\mu/kT = 0.55$, the interface width of the anisotropic surface becomes higher than that of the isotropic surface.

Another interesting result of the dynamics simulations for type I surfaces is that, at the supersaturation at which the sticking fraction becomes approximately linear, a maximum in the specific heat $c(\Delta\mu)$ is found for the case $\delta < 1$. The corresponding supersaturations were $\Delta\mu/kT = 0.7$ ($\delta = 0.8$), $\Delta\mu/kT = 0.9$ ($\delta = 0.6$) and $\Delta\mu/kT = 1.1$ ($\delta = 0.4$). In the case of type II surfaces, the situation is somewhat different. The attachment energies are equivalent for both surfaces (A or B on top). On the basis of the attachment energy criterion, the growth rate should be the same independent of the anisotropy. In Fig. 10, the sticking fraction is plotted *versus* the supersaturation for a temperature $kT/\Phi = 0.83$. It can be concluded that the anisotropy has the same kind of influence on the nucleation barrier as it has for type I faces. The shape of the curves, however, is different. Still, as for type I surfaces, the sticking fraction becomes almost immediately linear when growth starts for the almost isotropic case ($\delta = 0.8$). For the type II surface, the growth behaviour was also studied at temperatures near the maximum in the specific heat (in equilibrium). It appeared that the nucleation barrier becomes very small at temperatures above $T(c^{\max})$ (Fig. 11). This is in correspondence with the step-energy densities (Fig. 8) which drop to very low values at this temperature. This behaviour of the step energy as a function of temperature was found for both type I and type II surfaces. A remarkable feature of the anisotropic surfaces is that, at the supersaturation at which the sticking fraction becomes more or less linear, the interface width is very small indicating that the surface is still flat. Generally, it was not possible to derive a simple nucleation model which describes the MC results for the anisotropic type I and type II surfaces. These models are probably too simplified to

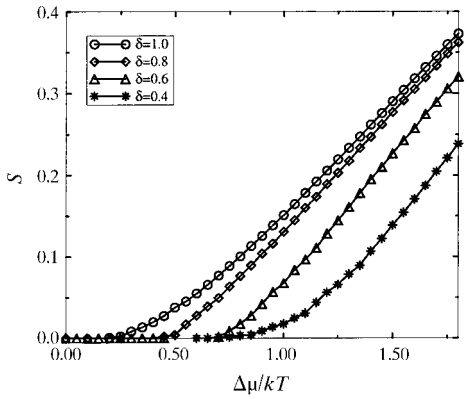

Fig. 9. Sticking fraction S for type I surfaces as a function of the supersaturation $\Delta\mu/kT$ at a temperature of $kT/\Phi = 0.83$ and for different anisotropies δ.

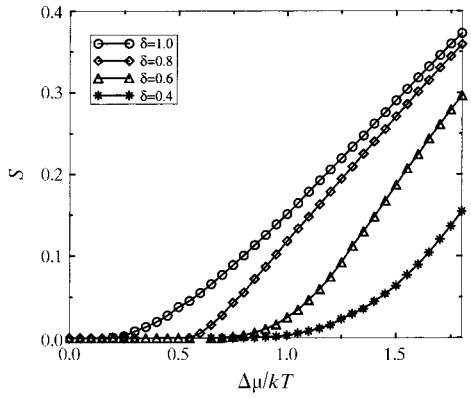

Fig. 10. Sticking fraction S for type II surfaces as a function of the supersaturation $\Delta\mu/kT$ for a temperature $kT/\Phi = 0.83$ and different anisotropies δ.

capture the essential kinetics of these more complicated surfaces as compared with the (001) faces of a Kossel crystal.

4.3.2. *Type III*. The results for type III surfaces are described in detail by Grimbergen, Meekes, Bennema, Knops & den Nijs (1998). In Fig. 12, the sticking fraction *versus* supersaturation is plotted for these types of surface. The temperature of $kT/\Phi = 0.67$ was chosen just below the pre-roughening temperature for the surface with $\delta = 0.8$ (Table 2). It has already been concluded from the connected-net analysis presented in §3 that the step free energy along the [010] direction is zero for $\delta = 1.0$. This is reflected in the absence of a nucleation barrier for $\delta = 1.0$. With decreasing δ, the step energy increases and thus the nucleation barrier increases. For this type of surface, the surface energy is directly related to the step energy. When δ increases, the surface energy of the most favourable surface (A or B) decreases. In terms of attachment energy, this implies that the growth rate will decrease for the face. This is in agreement with the MC simulation data (Fig. 12). It can be shown that at temperatures above the pre-roughening temperature T^{pr} this type of face still grows layer-by-layer at low supersaturations (Grimbergen, Meekes, Bennema, Knops & den Nijs, 1998). This result was also found for type IV surfaces as explained in the following section. The general behaviour of the sticking fraction clearly deviates from that of the type I and II surfaces. Only for the very anisotropic $\delta = 0.4$ surface, which corresponds to step energies Φ for steps along [010] and 0.86Φ for steps along [100], is the effective anisotropy very small in the sense that this surface behaves like a type I isotropic surface. For this case, the sticking fraction becomes indeed linear while for higher values of δ the sticking fraction saturates at lower supersaturations to the maximum value of approximately 0.5, which is determined by the SOS condition.

4.3.3. *Type IV*. In Fig. 13, the sticking fraction is plotted *versus* supersaturation for a type IV surface with $\delta = 0.6$ at different temperatures. From the equilibrium simulations, it was found that the pre-roughening temperature T^{pr} for this surface is $kT^{pr}/\Phi = 0.67$. Looking at Fig. 13, it is clear that for temperatures $T > T^{pr}$ there is still a significant nucleation barrier and the sticking fraction is clearly not linear for these temperatures. It is expected that at these temperatures the crystal face will grow as a flat face by a layer-by-layer mechanism. This is confirmed by the analysis of the average height of the surface [see equation (14)] as a function of time (Fig. 14). It appears that the surface grows with double layers AB (or BA) as expected from the connected-net analysis. The behaviour of the interface width for these types of surface is also remarkable. The values stick for a rather broad range of $\Delta\mu/kT$ at a value of unity and subsequently deviate slowly to higher values. The supersaturation at which the interface width starts to deviate from unity coincides with the supersaturation at which the sticking fraction becomes linear. In our opinion, the simulation data suggest that kinetic roughening may occur for this type of crystal face, but at rather high supersaturations. This can be attributed to

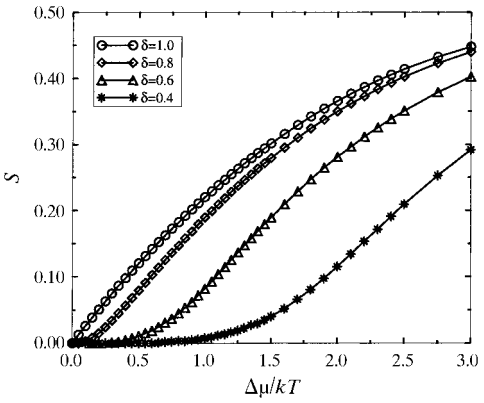

Fig. 12. Sticking fraction *versus* supersaturation for type III surfaces at $kT/\Phi = 0.67$.

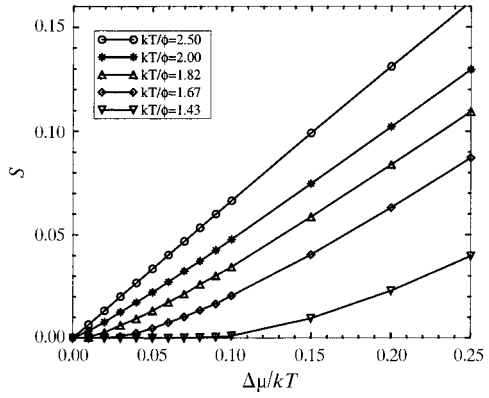

Fig. 11. Sticking fraction S for type II surfaces as a function of the supersaturation $\Delta\mu/kT$ for $\delta = 0.6$ and different temperatures $\{kT/\Phi\ [c(T)^{max}] = 1.90\}$.

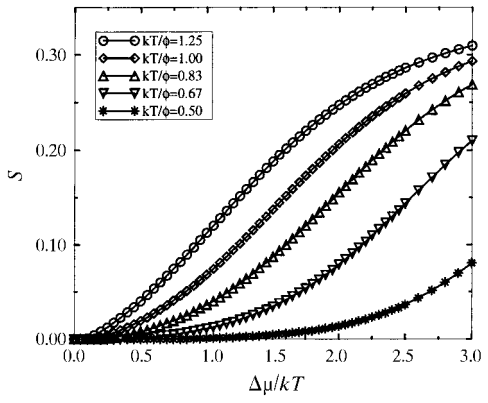

Fig. 13. Sticking fraction *versus* supersaturation for a type IV surface with $\delta = 0.6$ at different temperatures $[kT(c^{max})/\Phi = 0.67]$.

the strict SOS restriction that is applied which causes a decrease in available sites for attachment at the interface as the roughness increases. In contrast, the number of available sites for attachment of type I and II surfaces does not depend on the surface roughness.

5. Implications for the morphology

In this section, the most widely used recipes to determine the relative growth rates of crystal faces (R_{hkl}) will be discussed and compared with the MC simulation results.

A well known purely geometrical recipe for the relative growth rate R_{hkl} is given by

$$R_{hkl} \propto 1/d_{hkl}, \tag{15}$$

where d_{hkl} is the interplanar distance for a face (hkl) corrected for the X-ray reflection conditions given by Bravais, Friedel, Donnay and Harker (BFDH) (Donnay & Harker, 1937; Friedel, 1911). We will refer to this method as the BFDH method. The success of this simple recipe can be attributed to the fact that, for isotropic crystals, faces with a large d_{hkl} have a large energy content and are, therefore, the most stable faces.

A recipe that is taking the energy of a face into account is the frequently used attachment energy method. The attachment energy is defined as the energy released when a complete growth layer attaches to the surface. The attachment energy is related to the crystal energy by $E^{\rm cr} = E^{\rm sl}_{hkl} + E^{\rm att}_{hkl}$, where $E^{\rm sl}_{hkl}$ is the slice energy. Hartman & Bennema (1980) argued that for moderate supersaturations the relative growth rates may be obtained by

$$R_{hkl} \propto E^{\rm att}_{hkl}. \tag{16}$$

In the attachment-energy method, the interplanar distances are also corrected for the X-ray reflection conditions. Note that neither in the BFDH recipe nor in the attachment energy do the temperature or supersaturation play a role.

In this section, the crystal graph shown in Fig. 2 will be used to demonstrate that the above-mentioned recipes may lead to a very poor prediction of the growth morphology. It is assumed that the A and B growth units are chemically equivalent, but oriented differently. The space-group symmetry is supposed to be $Pmm2$. All connected nets were determined using the program *FACELIFT* (Grimbergen *et al.*, 1997). The connected forms found, with the number of different connected nets in parentheses, are {100} (1), {010} (2), {001} (2) and {011} (1). The predicted morphologies based on equations (15) and (16) are shown in Fig. 15. Note that the bond energies used to calculate the attachment energies are defined according to relation (7) which guarantees a constant lattice energy for different δ. As a result, the attachment energy for the {100}, {010} and {011} faces is equal to 2Φ and independent of δ. In contrast, the attachment energy for the {001} faces does depend on the anisotropy δ and is equal to $2\Phi_1$ (for $\Phi_1 < \Phi_2$) or $2\Phi_2$ (for $\Phi_1 > \Phi_2$) [compare Figs. 15(*c*) and (*d*)].

From Figs. 15(*a*) and (*b*), it can be observed that for this crystal graph there is already a large difference between the forms predicted using the BFDH or attachment-energy recipe. This difference can be attributed to the special bond topology at the surfaces, which is Kossel-like for the {110} and {100} faces and Kossel (110)-like for the {001} and {010} faces. Using the concept of symmetry roughening and pseudo-symmetry roughening, it is possible to modify the attachment-energy prediction by removing the faces that show symmetry roughening or pseudo-symmetry roughening

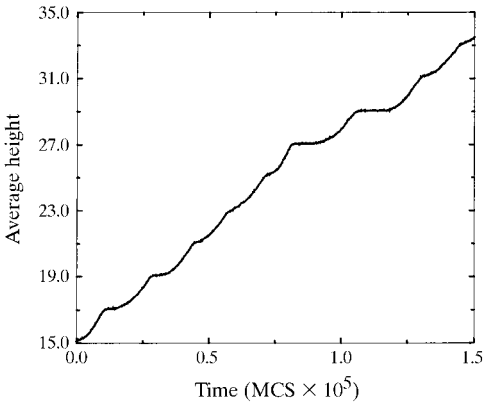

Fig. 14. The average height of the matrix (size $L = 40$) *versus* simulation time for type IV surfaces at $kT/\Phi = 0.83$ and $\Delta\mu/kT = 0.3$ ($kT^{\rm pr}/\Phi = 0.67$).

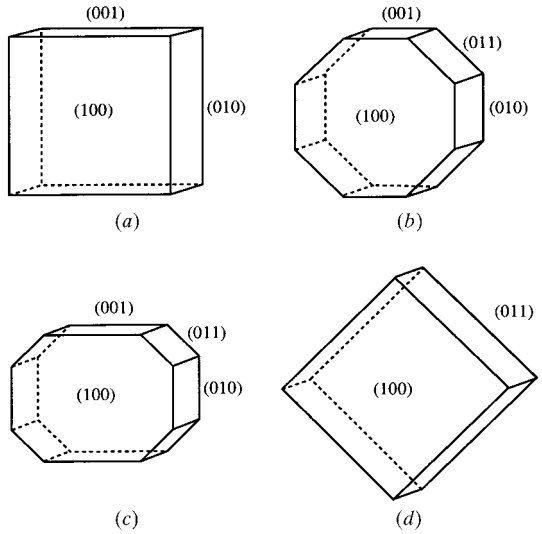

Fig. 15. Predicted growth morphology for the model graph of Fig. 2 based on (*a*) $R_{hkl} \propto 1/d_{hkl}$, (*b*) $R_{hkl} \propto E^{\rm att}_{hkl}$ ($\delta = 1.0$), (*c*) $R_{hkl} \propto E^{\rm att}_{hkl}$ ($\delta = 0.4$) and (*d*) $R_{hkl} \propto E^{\rm att}_{hkl}$ assuming that the {010} and {001} faces are symmetry roughened and have grown out.

from the morphology (see Fig. 15*d*). A better way to predict the growth morphology is to derive the relative growth rates directly from the MC simulations. For the simulations, it was assumed that the {100} and {011} faces can be modelled by an isotropic type I ($\delta = 1$) surface, whereas the {001} and {010} faces were modelled by a type III surface with $\delta = 0.8$ and $\delta = 1$, respectively. This is reasonable as an anisotropy of $\delta = 0.8$ has by far the most prominent effect on the faces {001} and {010}. The simulations were performed at a temperature of $kT/\Phi = 0.67$. In Fig. 16, the growth rates are plotted as a function of supersaturation. Owing to the assumption that both the {100} and {011} faces can be modelled with an isotropic type I surface, the ratio R_{100}/R_{011} is equal to the ratio of the interplanar distances d_{100}/d_{011}. The ratios R_{001}/R_{100} and R_{001}/R_{011} change as a function of supersaturation owing to the difference in surface bonding topology. According to the simulation data, the crystal habit will be bounded by {100} and {011} at low supersaturations ($\Delta\mu/kT < 1.25$). For supersaturations $\Delta\mu/kT > 1.25$, the {001} and {010} faces appear as well. Notice, however, that the {010} faces are rough owing to symmetry roughening. Therefore, if these faces appear, they will be rounded-off. Ultimately, at very high supersaturations, the morphology becomes isotropic and all orientations appear. This situation is, however, reached at a supersaturation at which all faces will be kinetically rough and the morphology will be sphere-like. Moreover, in practice this situation may never be reached as, at such high supersaturations, growth is mainly determined by mass transport limitations which are not present in our simulation model. Therefore, the results for high supersaturations probably represent a situation that will not be encountered in practice.

6. Discussion and conclusions

For type I and II faces, two phases could be identified, namely a flat phase and a rough phase. The effective step energy seems to be governed by the strongest connected net as presented in §3. From this connected net, the temperature at which the step energy becomes very small can be estimated by calculation of the two-dimensional Ising transition temperature T^C. The exact roughening transition temperature at equilibrium, however, is in most cases much higher than the calculated value of the strongest connected net. The two-dimensional Ising transition temperature based on the step energy of a complete step (001) seems to give a rather good estimate for the roughening transition temperature T^R. From the growth simulations, it can be concluded that two-dimensional nucleation growth is mainly determined by the step energy.

For type III surfaces, the step energy is determined by a difference in bond energies ($\Phi_p - \Phi_q$, Fig. 5). Therefore, the assumption that the step energy (and roughening temperature) is determined by the strongest connected net present for the orientation does not hold. Moreover, a special surface phase called a disordered flat phase was found (see Grimbergen, Meekes, Bennema, Knops & den Nijs, 1998). In our opinion, the step energy becomes very small at $T = T^{\mathrm{pr}}$ and therefore the nucleation barrier is very small. MC growth simulations confirm this behaviour, but it is very difficult to determine the supersaturation at which kinetic roughening occurs.

Type IV faces show a maximum in the specific heat at a temperature that coincides with calculated two-dimensional Ising transition temperatures based on the effective step energies for the surface. At that temperature, the step energies become almost zero, but the height-difference correlation function indicates that the surface is still not rough. It appears that this type of face does not show a roughening transition at finite temperatures. Similar behaviour was found for the staggered BCSOS model by Mazzeo *et al.* (1995). This is probably a result of the very strict SOS condition. Under growth conditions, it can be shown that the nucleation barrier has not disappeared at temperatures $T > T^{\mathrm{pr}}$. Moreover, the interface width indicates that the surface, even at rather high supersaturations, is still relatively flat. The dynamics of these types of surface need to be studied in more detail in order to understand the nucleation and growth behaviour of these types of crystal face.

The MC simulation data and the connected net analyses show that the assumption that rough faces have a high growth rate compared with macroscopically flat growing faces is not generally valid. The growth rate does depend on both the step energy and the surface energy (or attachment energy) of a crystal face. In the case of the presence of a DOF phase, it appears that faces can have a very high growth rate and still be macroscopically flat. Experimental examples of such

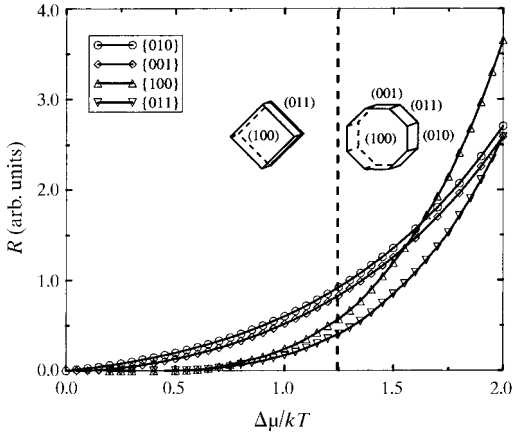

Fig. 16. Growth rates R as a function of supersaturation for the {100}, {011}, {001} and {010} faces of the crystal graph of Fig. 2.

growth behaviour were found for the (011) face of naphthalene (Grimbergen, Reedijk *et al.*, 1998), the (110) faces of orthorhombic *n*-paraffins (Grimbergen, van Hoof *et al.*, 1998), the top faces of triacylglyceride (fat) crystals (Hollander *et al.*, 1999) and the (110) faces of lysozyme (Grimbergen *et al.*, 1999).

In this paper, it is shown that the BFDH and attachment-energy predictions are not generally applicable as the predictive value seems to be very poor even for many practical crystal graphs, when compared with the results of a complete connected-net analysis and MC simulation data. The simulation data clearly demonstrate that the morphology often depends very strongly on the temperature and supersaturation. The latter phenomenon is encountered frequently in the practice of crystal growth, although the usual methods for predicting the crystal morphology do not take it into account.

The results of the present paper indicate that it is very important to study the exact bonding topology in order to predict surface phase transitions and growth kinetics. The connected-net analysis yields important information that can be used to predict the equilibrium and growth behaviour qualitatively. Moreover, for crystals with a complex bonding structure, the connected-net analysis offers a tool to categorize the many connected nets often present for a single orientation (*hkl*) into relatively simple models of surfaces of the types treated in the present paper. For the future, the combination of a connected-net analysis, MC simulations and statistical thermodynamical surface models appears to be a powerful tool in predicting and understanding not only the equilibrium but also the growth behaviour of crystal faces quantitatively.

RFPG would like to acknowledge the financial support of the Dutch Technology Foundation (STW).

References

Beijeren, H. van (1977). *Phys. Rev. Lett.* **38**, 993–996.
Beijeren, H. van & Nolden, I. M. (1986). *Topics in Current Physics, Structure and Dynamics of Surfaces II*, Vol. 43, pp. 259–300. Berlin: Springer Verlag.
Donnay, J. D. H. & Harker, D. (1937). *Am. Mineral.* **22**, 446–467.
Follner, H. (1988). *Fortschr. Miner.* **66**, 37–68.
Friedel, G. (1911). *Leçon de Cristallographie.* Paris: Hermann.
Gilmer, G. H. & Jackson, K. A. (1977). *1976 Crystal Growth and Materials*, edited by E. Kaldis & H. J. Scheel. Amsterdam: North Holland.
Grimbergen, R. F. P., Boek, E. S., Meekes, H. & Bennema, P. (1999). To be published.
Grimbergen, R. F. P., van Hoof, P. J. C. M., Meekes, H. & Bennema, P. (1998). *J. Cryst. Growth.*, **191**, 846–860.
Grimbergen, R. F. P., Meekes, H., Bennema, P., Knops, H. J. F. & den Nijs, M. (1998). *Phys. Rev. B*, **58**, 5258–5268.
Grimbergen, R. F. P., Meekes, H., Bennema, P., Strom, C. S. & Vogels, L. J. P. (1998). *Acta Cryst.* A**54**, 491–500.
Grimbergen, R. F. P., Meekes, H. & Boerrigter, S. X. M. (1997). *C-Program FACELIFT for Connected Net Analysis.* Department of Solid State Chemistry, University of Nijmegen, The Netherlands.
Grimbergen, R. F. P., Reedijk, M. F., Meekes, H. & Bennema, P. (1998). *J. Phys. Chem.* B**102**, 2646–2653.
Hartman, P. & Bennema, P. (1980). *J. Cryst. Growth*, **49**, 145–156.
Hoeks, B. (1993). *C-Program TCRITIC. Program for Calculating Ising Transition Temperatures.* Department of Solid State Chemistry, University of Nijmegen, The Netherlands.
Hollander, F. F. A., Grimbergen, R. F. P., Boerrigter, S. X. M., van de Streek, C. J., Meekes, H. & Bennema, P. (1999). To be published.
Leamy, H. J. & Gilmer, G. H. (1974). *J. Cryst. Growth*, **24/25**, 499–502.
Mazzeo, G., Carlon, E. & Beijeren, H. van. (1995). *Phys. Rev. Lett.* **74**, 1391–1395.
Meekes, H., Bennema, P. & Grimbergen, R. F. P. (1998). *Acta Cryst.* A**54**, 501–510.
Nijs, M. den (1997). *J. Phys. A*, **30**, 397–404.
Nijs, M. den & Rommelse, K. (1989). *Phys. Rev. B*, **40**, 4709–4734.
Nolden, I. M. & van Beijeren, H. (1994). *Phys. Rev. B*, **49**, 17224.
Rommelse, K. & den Nijs, M. (1987). *Phys. Rev. Lett.* **59**, 2578–2581.
Shugard, W. J., Weeks, J. D. & Gilmer, G. H. (1978). *Phys. Rev. Lett.* **41**, 1399–1402.
Swendsen, R. H. (1977). *Phys. Rev. B*, **15**, 5421–5431.
Weeks, J. D. (1986). *Ordering in Strongly Fluctuating Condensed Matter Systems*, edited by T. Riste, p. 293. New York: Plenum Press.
Woodraska, D. L. & Jaszczak, J. A. (1997*a*). *Phys. Rev. Lett.* **78**, 258–261.
Woodraska, D. L. & Jaszczak, J. A. (1997*b*). *Surf. Sci.* **374**, 319–332.